

### Numerical Heat Transfer, Part A: Applications



Date: 05 July 2017, At: 08:05

ISSN: 1040-7782 (Print) 1521-0634 (Online) Journal homepage: http://www.tandfonline.com/loi/unht20

# INFLUENCE OF WALL CONDUCTION ON MIXED CONVECTION HEAT TRANSFER IN EXTERNALLY FINNED PIPES

F. Moukalled, M. Darwish & S. Acharya

To cite this article: F. Moukalled, M. Darwish & S. Acharya (1995) INFLUENCE OF WALL CONDUCTION ON MIXED CONVECTION HEAT TRANSFER IN EXTERNALLY FINNED PIPES, Numerical Heat Transfer, Part A: Applications, 28:2, 157-173, DOI: 10.1080/10407789508913739

To link to this article: <a href="http://dx.doi.org/10.1080/10407789508913739">http://dx.doi.org/10.1080/10407789508913739</a>

	Published online: 02 Mar 2007.
	Submit your article to this journal 🗗
ılıl	Article views: 14
a a	View related articles 🗹
4	Citing articles: 2 View citing articles 🗗

Full Terms & Conditions of access and use can be found at http://www.tandfonline.com/action/journalInformation?journalCode=unht20

## INFLUENCE OF WALL CONDUCTION ON MIXED CONVECTION HEAT TRANSFER IN EXTERNALLY FINNED PIPES

#### F. Moukalled and M. Darwish

Faculty of Engineering and Architecture, Mechanical Engineering Department, American University of Beirut, Beirut, Lebanon

#### S. Acharva

Mechanical Engineering Department, Louisiana State University, Baton Rouge, Louisiana 70803

The influence of wall heat conduction on laminar mixed convection in externally finned vertical pipes are investigated numerically. Buoyancy in both aiding and opposed modes is considered. Results are presented in terms of the streamwise variation of the fluid bulk temperature and tube-side Nusselt number, axially averaged and periodically fully developed Nusselt number values, and axial velocity and temperature profiles. For opposed flows, buoyancy forces decrease the overall heat transferred to the fluid, while for buoyancy-aided flows, buoyancy causes an enhancement in the overall heat transferred to the fluid. Inclusion of longitudinal wall conduction increases the heat transfer to the fluid and enhances the effects of buoyancy.

#### INTRODUCTION

The present study attempts to determine the influence of pipe wall thermal conductivity on the hydrodynamic and thermal characteristics of mixed convection heat transfer in longitudinally conducting, externally finned, vertical pipes. Externally finned pipes are extensively used in heat exchange applications. The equally spaced annular or square fins on the outer surface of the pipe (Figure 1a) act as local enhancement devices, augmenting heat transfer to or from the finned pipe by increasing the local heat transfer surface area. Therefore, if the increase in the pipe area over a finned section is treated as an increase in the heat transfer coefficient, then the outer surface of the finned pipe may be assumed to be subjected to spatially periodic boundary conditions with low heat transfer coefficient ( $h_t$ ) along the unfinned sections and high heat transfer coefficient ( $h_t$ ) along the finned sections. A schematic of the above-described model for the variation of

Received 7 June 1994; accepted 27 December 1994.

The financial support provided by the University Research Board of the American University of Beirut through grant 113040-48816 is gratefully acknowledged.

Address correspondence to Dr. Surmanta Acharya, Department of Mechanical Engineering, Louisiana State University, Baton Rouge, LA 70803-6413, USA.

	NOMENCLATURE									
Bi	Biot number $(=hR_i/k)$	x, X	dimensional and dimensionless							
Bi <sub>n</sub>	average Biot number $[=(\sigma Bi_n +$		axial coordinate $[=x/(R_i Pe)]$							
_	$\tau \operatorname{Bi}_{f}/(\sigma+\tau)$	α	parameter in Eq. (5) $\{=2 \text{ Pe}^2/$							
Bi <sub>u</sub> , Bi <sub>f</sub>	Biot numbers for the unfinned		$[(R_0/R_i)^2-1]$							
	and finned regions	β	coefficient of thermal expansion							
8	gravitational acceleration	γ	parameter in Eq. (5) $\{ = \alpha [Bi -$							
Gr	Grashof number $[=g\beta(T_{\infty} -$		$\kappa(\partial\theta/\partial\eta)_{n-1}$							
	$T_{\rm in})R_{\rm i}^3/\nu^2$	η	dimensionless radial coordinate							
h	heat transfer coefficient		$(=r/R_i)$							
k	thermal conductivity	θ	dimensionless temperature							
$L_{\rm p}$	tube length		$[=(T-T_{\rm in})/(T_{\rm o}-T_{\rm in})]$							
N	north neighbor of the P grid point	K	fluid to wall thermal conductivity							
Nu	local Nusselt number		ratio $(=k_{fl}/k_{w})$							
Nu <sub>u</sub> , Nu <sub>f</sub>	Nu values over the unfinned and	ν	kinematic viscosity							
	finned regions	ρ	density							
$\overline{Nu}_{u}, \overline{Nu}_{f}$	Average Nu values over the	$\sigma$	dimensionless interfin spacing							
,	unfinned and finned regions		$[=s/(R_i Pe)]$							
Nus	average Nusselt number	au	dimensionless fin thickness							
P	pressure		$[=t/(R_{\rm i}{\rm Pe})]$							
P	dimensionless pressure; also	φ	dependent variable							
	main grid point	$\psi$	stream function							
Pe	Péclet number	ω	dimensionless radial coordinate							
Pr	Prandtl number		$\{=[\psi - (\psi)_{\eta=0}]/[(\psi)_{\eta=1} -$							
Q	rate of heat transfer between		$(\psi)_{n=0}$ ]							
	x = 0 and $x = x$		•							
r	radial coordinate	Subscri	pts							
$R_{\rm i}$	inner radius of pipe									
r	radial coordinate	a	average value							
$R_{\rm i}$	inner radius of pipe	bx	refers to bulk temperature at any							
•	outer radius of pipe		x location							
Re	Reynolds number $(= \rho u_a R_i/\mu)$	f	finned section							
S	interfin spacing	in	condition at inlet							
S	south neighbor of the P grid point	max	maximum value							
t	fin thickness	pd	periodically fully developed							
T	dimensional temperature	u	unfinned section							
u, U	dimensional and dimensionless	WX	refers to wall condition at any							
	axial velocity $(= u/u_a)$		x location							
u <sub>a</sub>	average axial velocity	œ	ambient condition							

the heat transfer coefficient along the finned and unfinned sections of the pipe is shown in Figure 1b.

Studies on forced convection heat transfer in externally finned pipes are limited to those reported in Refs. [1-3]. Sparrow and Charmchi [1] analyzed the behavior of laminar forced convection heat transfer in externally finned pipes but neglected the effect of axial conduction in the pipe wall. Moukalled and Acharya [2] and Moukalled et al. [3] extended the work reported by Sparrow and Charmchi [1] and studied the effect of conduction in the pipe wall for laminar and turbulent flow situations, respectively. The significant influence of axial wall conduction on the heat transfer behavior was clearly demonstrated. In a recent paper, Moukalled

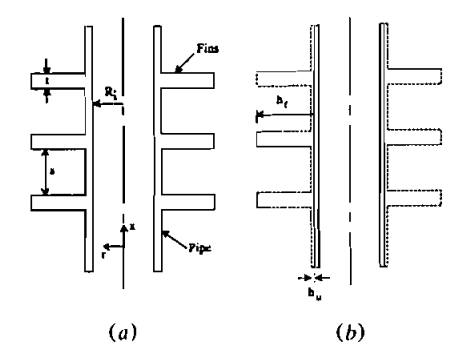


Figure 1. (a) Physical situation for the externally finned pipe. (b) Adopted model for the variation of the external heat transfer coefficient.

et al. [4] studied the influence of buoyancy forces on forced convection heat transfer in vertically oriented, externally finned pipes, but they neglected axial conduction in the pipe wall.

A number of analytical and numerical studies on conjugate forced convection heat transfer in smooth pipes have also been reported [5-11]. These studies have clearly established the importance of conjugate heat transfer.

Several researchers have also investigated the effects of buoyancy on forced convection heat transfer in smooth circular tubes. Conjugate effects have also been considered. The work reported in Refs. 12–16 neglected axial conduction in the pipe wall and dealt with mixed convection heat transfer in circular pipes. Heggs et al. [17] studied the effects of conduction in the pipe wall on the development of recirculating mixed convection flows in isothermal vertical pipes. Bernier and Baliga [18] extended the work of Heggs et al. [17] for uniformly heated pipes.

The objective of this article is to extend the work reported in Ref. [4] and to present numerical solutions for laminar mixed convection heat transfer in externally finned, conducting vertical pipes. Both aiding and opposed mixed convection situations are considered. Radial conduction in the pipe wall is neglected, and therefore, results are valid for relatively thin pipes. The coupling between mixed convection in the pipe and conduction in the pipe wall is accomplished by ensuring continuity of the thermal conditions along the inside surface of the pipe. Since these conditions are solution dependent, an iterative solution procedure has to be adopted. Furthermore, due to lack of numerical and experimental data for the problem, comparison is made with predictions obtained for an unfinned tube and with those calculated with the spatially averaged values of the high and low external Biot numbers.

#### **GOVERNING EQUATIONS**

The problem considered is shown schematically in Figure 1a and involves the flow and heat transfer in a vertically oriented, longitudinally conducting, externally finned circular pipe. The model used to describe the variation of the heat transfer coefficient on the outer surface of the pipe is depicted in Figure 1b. The flow is assumed to be steady, laminar, and two-dimensional. The finned section is assumed to be preceded by a long unheated pipe, so that at the inlet, Poiseuille flow can be

assumed. Buoyancy effects in the finned pipe will accelerate the flow in the aiding mode and decelerate the flow in the opposing mode. Density variation is modeled by using the Boussinesq approximation. For small and moderate temperature differences, the Boussinesq assumption has been shown to be adequate. Radiation effects are assumed to be small.

To minimize the number of parameters, the following dimensionless variables are introduced:

$$X = \frac{x}{R_i \text{ Pe}} \qquad \eta = \frac{r}{R_i} \qquad U = \frac{u}{u_a} \qquad V = \frac{v}{u_a/\text{Pe}}$$

$$P = \frac{p + \rho gx}{\rho u_a^2} \qquad \theta = \frac{T - T_{\text{in}}}{T_{\infty} - T_{\text{in}}}$$
(1)

Since the Péclet number range of interest here is larger than 50, the axial diffusion of momentum and energy in the fluid is neglected. Thus the flow is of the parabolic or boundary layer type.

With the aforementioned assumptions and dimensionless variables, the fluid nondimensional momentum and energy equations become

$$U\frac{\partial U}{\partial X} + V\frac{\partial U}{\partial \eta} = -\frac{\partial P}{\partial X} + \Pr \frac{1}{\eta} \frac{\partial U}{\partial \eta} \left( \eta \frac{\partial U}{\partial \eta} \right) + \frac{\operatorname{Gr} \operatorname{Pr}}{\operatorname{Re}} \theta \tag{2}$$

$$U\frac{\partial\theta}{\partial X} + V\frac{\partial\theta}{\partial\eta} = \frac{1}{\eta}\frac{\partial}{\partial\eta}\left(\eta\frac{\partial\theta}{\partial\eta}\right) \tag{3}$$

Since Eqs. (2) and (3) are parabolic in nature, hydrodynamic and thermal boundary conditions are needed along X=0 and along  $\eta=0$  and  $\eta=1$ . These conditions can be expressed as

$$U = 2(1 - \eta^2)$$
  $\theta = 0$  at  $X = 0$  (4a)

$$\frac{\partial U}{\partial n} = 0$$
  $\frac{\partial \theta}{\partial n} = 0$  at  $\eta = 0$ ;  $U = 0$   $\theta = \theta_{\rm w}(X)$  at  $\eta = 1$  (4b)

In Eq. (4b),  $\theta_{\rm w}$  represents the pipe wall temperature, which is not known beforehand, but is determined from the solution. Discussion on how the correct solution for  $\theta_{\rm w}$  is obtained is given in the next section.

The equation for the pipe wall temperature is derived from a quasi-onedimensional energy balance on a control volume along the wall of the pipe. Its final dimensionless form may be expressed as

$$\frac{\partial^2 \theta_{\rm w}}{\partial X^2} - \alpha \operatorname{Bi} \theta_{\rm w} + \gamma = 0 \tag{5}$$

where

$$\alpha = \frac{2 \operatorname{Pe}^2}{\left(R_0 / R_i\right)^2 - 1} \qquad \gamma = \alpha \left[ \operatorname{Bi} - \kappa \left( \frac{\partial \theta}{\partial \eta} \right)_{\eta = 1} \right] \qquad \kappa = \frac{k_{\text{fl}}}{k_{\text{w}}} \tag{6}$$

In the above equation, Bi is the Biot number, which varies periodically on the outer surface of the pipe and is equal to Bi<sub>u</sub> along the unfinned portion,  $n(\sigma + \tau) < X < n(\sigma + \tau) + \sigma$ , and Bi<sub>f</sub> along the finned portion  $n(\sigma + \tau) + \sigma < X < (n + 1)(\sigma + \tau)$ , respectively.

Thermal boundary conditions are needed in order to solve the equation for pipe wall heat conduction (Eq. (5)). Due to lack of better information, it is assumed that poorly conducting pipes (e.g., a CPCV pipe) are connected upstream and downstream of the externally finned pipe section. Such boundary conditions have also been used by many other workers [2, 3, 5, 6]. Mathematically, the boundary conditions can be written as

$$\frac{\partial \theta_{\mathbf{w}}}{\partial X} = 0 \quad \text{at} \quad X = 0 \qquad X = L_{\mathbf{p}} \tag{7}$$

Another reasonable boundary condition at X=0 is to assume that the fluid and pipe wall are in thermal equilibrium, i.e.,  $\theta_{\rm w}=0$  at X=0. This is justified by the fully developed velocity profile (parabolic) used at the inlet (X=0). Computations using this boundary condition have also been obtained, but for few cases only, and are used for comparison.

It should be pointed out that the term  $(\partial\theta/\partial\eta)_{\eta=1}$  appearing in Eq. (6) is the dimensionless heat flux leaving the pipe wall from the fluid side and provides the coupling between the fluid and the pipe wall temperatures. Since it is not known a priori to the calculation, it has to be determined in the course of the solution.

#### SOLUTION PROCEDURE AND COMPUTATIONAL DETAILS

In contrast to earlier conjugate heat transfer computations reported in Refs. [2, 3], the flow and temperature fields in the present problem are intimately coupled by the body force term appearing in the momentum equation. Therefore, the fluid velocity and energy equations have to be solved simultaneously. The solution is determined using an implicit finite difference method, due to Patankar and Spalding [19], that starts at the inlet to the finned pipe section and proceeds step by step until the exit is reached. The finite difference equations are obtained by integrating the differential equations over a control volume in the flow and using profile approximations in each coordinate direction (the power law scheme is used here [20]). Owing to the parabolic nature of the differential equations, the algebraic equation at a typical grid point P at a streamwise location  $X_D$  has a tridiagonal form that is solved directly by the Thomas algorithm [20].

The discretized form of the one-dimensional wall conduction equation (Eq. (5)) is obtained using the control volume approach of Patankar [20] and the central difference scheme. Again, a system of tridiagonal equations is obtained that is solved directly by the Thomas algorithm [20].

The overall solution procedure is iterative in nature and consists of repeatedly solving the momentum and energy equations for the fluid and the conduction equation for the pipe wall. Iterations start by solving the fluid momentum and energy equations, from pipe inlet to pipe exit, using a guessed value for  $\theta_w(X)$  needed as a boundary condition (Eq. (4b)) for Eq. (3). The resulting solution allows the calculation of the term  $(\partial\theta/\partial\eta)_{\eta=1}$  needed in solving the pipe wall conduction equation. After feeding this term into the wall conduction equation (Eq. (5)), this equation is solved to obtain updated values for  $\theta_w(X)$ . The new values of  $\theta_w(X)$  are used to initiate the next iteration, and the fluid momentum and energy equations are solved again. This procedure is continued until convergence to at least four significant figures is reached. Typically, three to eight iterations are needed.

Due to the periodic nature of the boundary condition on the outer surface, a dense grid system had to be used in order to resolve the new thermal boundary layer developing at each forward finned segment. The boundary layer calculations were performed with 100 cross-stream grid points and 90,000 forward steps, with step sizes ranging between  $10^{-6}$  at X=0 to  $10^{-5}$  at the exit. The cross-stream grid points were concentrated near the wall, where larger gradients are expected to be present. The grid point distribution was carefully tailored to provide grid-independent results. For the solution of the pipe wall conduction equation, 9150 grid points were used. The conduction control volume faces were chosen to be identical to streamwise positions in the flow solution in order to eliminate the need for interpolation in transferring information between the conduction and flow solutions.

The grid independence of the results is verified by obtaining results for a finer grid (200 cross-stream points) and comparing them with the results for the coarser grid (100 grid points). This comparison is shown in Figure 2, where the U velocity profiles at X=0.15 are plotted across the pipe. Also shown in Figure 2 are results obtained with a constant smaller forward step size of  $10^{-7}$  in the flow problem, and 18,300 grid points in the conduction problem. The two sets of results shown are nearly identical, confirming the adequacy of the grid used.

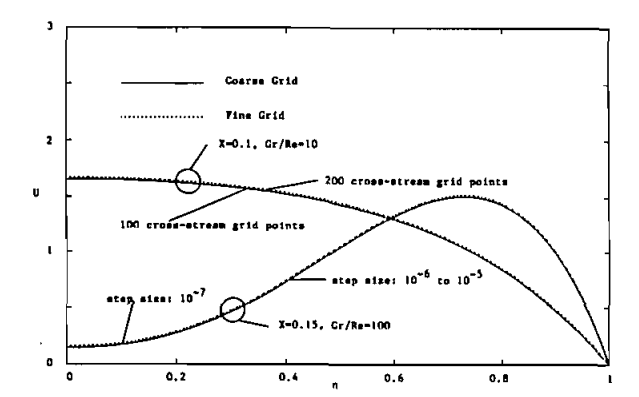


Figure 2. Comparison of velocity profiles at two different axial stations and for two distinct Gr/Re values, obtained using coarse and fine mesh systems ( $Bi_u = 1$ ,  $Bi_f = 50$ ,  $\tau = 10^{-4}$ ,  $\sigma = 3\tau$ , and  $\kappa = \infty$ ).

#### **RESULTS AND DISCUSSION**

Inspection of the dimensionless quantities reveals four geometric parameters: the inner to outer radius ratio  $(R_i/R_o)$ , which is fixed at 0.9 to simulate thin pipes; the dimensionless pipe length  $L_p$ , which is assigned the value of 0.3 (this value is 50% higher than the value reported in Refs. [1-3], within which the pure forced convection flow attains a thermally fully developed state); the interfin spacing  $\sigma$ ; and the fin thickness  $\tau$ . Furthermore, there are five thermal and hydrodynamic parameters, namely, the fluid to wall thermal conductivity ratio  $\kappa$ , the low and high Biots numbers (Bi, and Bi, respectively), the Prandtl number (Pr), and the ratio of Grashof to Reynolds numbers (Gr/Re). Parameter values chosen are two sets of low and high Biot numbers ( $Bi_u = 1$ ,  $Bi_f = 50$  and  $Bi_u = 5$ ,  $Bi_f = 250$ ), a dimensionless fin thickness  $\tau = 10^{-4}$ , two interfin spacing values ( $\sigma = 3\tau$  and  $7\tau$ ), four Gr/Re values (-10, 0, 10, and 100), and three values for the fluid to wall thermal conductivity ratio ( $\kappa = \infty$  representing the limiting case of no conduction in the pipe wall,  $\kappa = 16.5 \times 10^{-3}$  representing a pipe of low thermal conductivity, and  $\kappa = 1.65 \times 10^{-3}$  representing a pipe of high thermal conductivity). Water is chosen as the working fluid, and therefore Pr is assigned the value of 3.01 (corresponding to a reference temperature of 59.5°C).

As mentioned earlier, the purpose of this study is to highlight the effects of axial conduction in the pipe wall on mixed convection heat transfer in externally finned pipes. Therefore, the discussion presented will concentrate on the combined effects of pipe wall thermal conductivity and buoyancy forces on the heat transfer and flow field.

#### **BULK TEMPERATURES**

The fluid bulk temperature, which also represents the fraction of the maximum possible heat that can be transferred to the fluid and is, therefore, a measure of the degree of its relative thermal saturation, is defined as

$$\frac{Q}{Q_{\text{max}}} = \theta_{\text{bx}} = 2 \int_0^1 U\theta \eta \, d\eta \tag{8}$$

The streamwise variation of  $\theta_b$  (or  $Q/Q_{max}$ ) is presented in Figures 3-6. In Figures 3-5, results obtained with zero wall conductivity ( $\kappa = \infty$ ) [4] are compared with results obtained using finite wall conductivity ( $\kappa = 16.5 \times 10^{-3}$  and  $\kappa = 1.65 \times 10^{-3}$ ), for different values of Gr/Re. From these plots, it can easily be seen that, for all values of  $\kappa$ , the heat transfer rate increases with increasing positive values of Gr/Re (aided flow), and decreases for negative values of Gr/Re (opposed flow). Furthermore, at any value of Gr/Re, the heat transferred to the fluid increases significantly when longitudinal conduction along the pipe wall is accounted for. This behavior was also noted in the forced convection (Gr/Re = 0) study reported in Ref. [2].

Buoyancy effects are seen to be underestimated when the pipe wall thermal conductivity is not accounted for. For negative values of Gr/Re, since buoyancy opposes the forced flow, there is a decrease in heat transfer from the forced

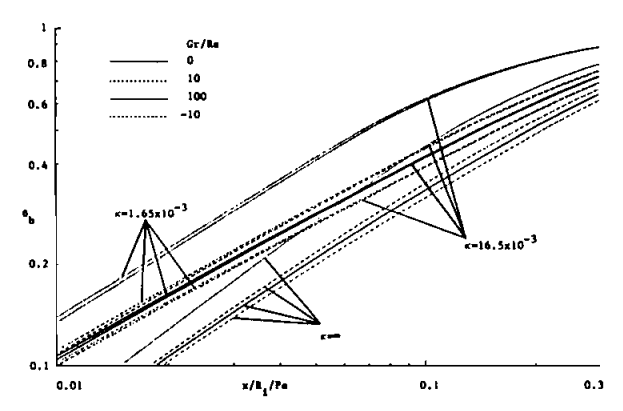


Figure 3. Streamwise variation of the bulk temperature  $\theta_b$  (or  $Q/Q_{max}$ ) for axially periodic Biot number values (Bi<sub>u</sub> = 1, Bi<sub>f</sub> = 50,  $\tau$  =  $10^{-4}$ , and  $\sigma$  =  $3\tau$ ).

convection value, and this decrease is seen to be smaller for a lower pipe wall conductivity. For  $\kappa = \infty$ , the percent decrease in the heat transferred to the fluid from the forced convection values is 3.17% at X = 0.01, 4.81% at X = 0.05, and 3.91% at the pipe exit. For  $\kappa = 16.5 \times 10^{-3}$  these percentages are 3.81%, 6.09%, and 4.02%, respectively, and for  $\kappa = 1.65 \times 10^{-3}$  the corresponding values are slightly higher. To explain this behavior, it should be noted that when conduction in the pipe wall is taken into consideration, the preheating of the pipe wall by conduction increases its upstream temperature, causing greater radial temperature differences that lead to stronger buoyancy-induced convection effects. Since for negative Gr/Re values, buoyancy opposes forced convection, stronger buoyancy due to wall conduction effects retards the flow further, and leads to a decrease in the heat transfer coefficient.

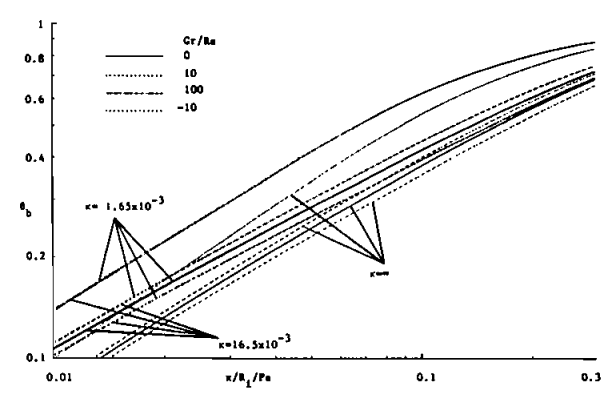


Figure 4. Streamwise variation of the bulk temperature  $\theta_b$  (or  $Q/Q_{\rm max}$ ) for axially periodic Biot number values (Bi<sub>u</sub> = 5, Bi<sub>f</sub> = 250,  $\tau = 10^{-4}$ , and  $\sigma = 3\tau$ ).

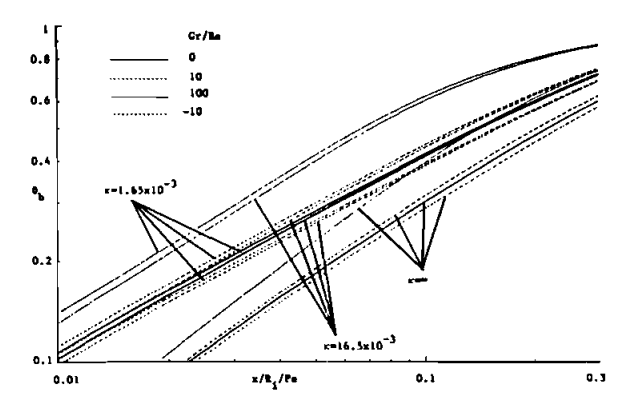


Figure 5. Streamwise variation of the bulk temperature  $\theta_b$  (or  $Q/Q_{\rm max}$ ) for axially periodic Biot number values (Bi<sub>u</sub> = 1, Bi<sub>f</sub> = 50,  $\tau = 10^{-4}$ , and  $\sigma = 7\tau$ ).

For positive values of Gr/Re, i.e., when Gr/Re = 10 or 100, the increase in heat transfer over the forced convection value is greater for higher values of pipe wall thermal conductivity. For Gr/Re = 100, the increase in heat transfer over the forced convection value for the nonconducting pipe is 14.28% at X = 0.01, 28.85% at X = 0.05, and 23.125% at the pipe exit. For  $\kappa = 16.5 \times 10^{-3}$  these percentages are 28.57%, 46.236%, and 22.3%, respectively, and for  $\kappa = 1.65 \times 10^{-3}$  the corresponding values are 29.63%, 47.35%, and 22.18%, respectively. In this situation, buoyancy aids the flow by accelerating it near the pipe wall and, thus, augments the convection heat transfer coefficient. When conduction in the pipe wall is accounted for, preheating by axial conduction increases the pipe wall temperatures upstream, causing greater radial temperature variations and stronger buoyancy-induced convection. Thus, the buoyancy-induced increase in heat transfer is higher at a higher wall thermal conductivity.

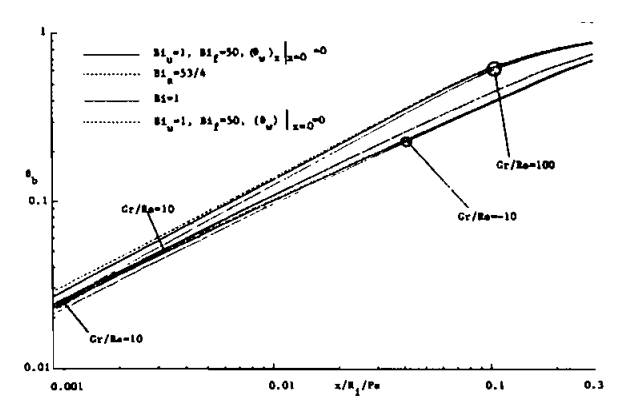


Figure 6. Streamwise variation of the bulk temperature  $\theta_b$  (or  $Q/Q_{\rm max}$ ) for axially periodic and constant Biot number values using two pipe wall boundary conditions (Bi<sub>u</sub> = 1, Bi<sub>f</sub> = 50,  $\tau = 10^{-4}$ ,  $\sigma = 3\tau$ , and  $\kappa = 16.5 \times 10^{-3}$ ).

For the aided flows, and particularly at the higher Gr/Re values, the increase in heat transfer over the forced convection values exhibits a small peak near the midstream location due to the buoyant acceleration of flow near the pipe wall that causes an increase in the tube-side convection heat transfer coefficient. As the flow develops further, and toward the fully developed condition, the rate of increase in heat transfer decreases toward the forced convection value.

The above stated trends and corresponding explanation apply to all cases presented in Figures 3-5. However, with increasing levels of the external heat transfer coefficients (compare Figure 3, for which  $\mathrm{Bi}_u=1$  and  $\mathrm{Bi}_f=50$ , and Figure 4, for which  $\mathrm{Bi}_u=5$  and  $\mathrm{Bi}_f=250$ ), the external thermal resistances are smaller, the wall temperatures are more uniform, and the influence of longitudinal pipe conduction is reduced. With increasing interfin spacing (compare Figure 3, for which  $\sigma=3\tau$ , and Figure 5, for which  $\sigma=7\tau$ ), the external convective resistance is higher, and consequently, the effect of pipe wall thermal conductivity is greater.

As mentioned earlier, two boundary conditions at X=0 are considered for the solution of the conduction equation, Eq. (5). The boundary condition used in obtaining the results presented in Figures 3-5 is the adiabatic condition  $\partial \theta_w / \partial X = 0$ . Limited calculations are also performed with the isothermal boundary condition  $\theta_w = 0$  at X=0. The comparison between the two boundary conditions for a typical case (Bi<sub>u</sub> = 1, Bi<sub>f</sub> = 50,  $\sigma = 3\tau$ , and  $\kappa = 16.5 \times 10^{-3}$ ) is shown for Gr/Re = 10 in Figure 6. It may be noted that the curve for the adiabatic boundary condition is very close to that for the isothermal boundary condition. The difference between the two curves is only near the entrance to the pipe, and after the initial entry region, the two curves merge into one.

Results are also compared in Figure 6 with corresponding unfinned tube results ( $\mathrm{Bi}_{\mathrm{u}}=1$ ) and with results obtained using a uniform area-averaged Biot number ( $\mathrm{Bi}_{\mathrm{a}}$ , defined in the nomenclature) suggested by Sparrow and Charmchi [1]. The extent to which the finned-tube lines lie above the  $\mathrm{Bi}=1$  lines indicates the degree of heat transfer enhancement achieved by finning. The constant lines corresponding to  $\mathrm{Bi}_{\mathrm{a}}$  lie slightly above the curves for the streamwise periodic cases, but the differences are not large (less than 10% at X=0) and decrease in the streamwise direction. Thus, for conducting pipes, in the absence of solutions for the periodic cases, heat transfer results corresponding to this type of  $\mathrm{Bi}_{\mathrm{a}}$  might be considered as a first approximation for those for a periodic  $\mathrm{Bi}$ . However, for the nonconducting case ( $\kappa=\infty$ ) the differences between the area-averaged bulk temperature and the true value are considerably larger (nearly 27% at X=0 for the parameters in Figure 6). Thus, the  $\mathrm{Bi}_{\mathrm{a}}$  approximation improves with increasing wall conductivity.

#### **NUSSELT NUMBERS**

The streamwise variations of the tube-side Nusselt numbers, defined as

$$Nu_{u} = \frac{h_{u}D}{k} \qquad h_{u} = \frac{\int_{\sigma} q \, dx}{\int_{\sigma} (T_{wx} - T_{bx}) \, dx} \qquad Nu_{f} = \frac{h_{f}D}{k} \qquad h_{f} = \frac{\int_{\tau} q \, dx}{\int_{\tau} (T_{wx} - T_{bx}) \, dx}$$

$$\tag{9}$$

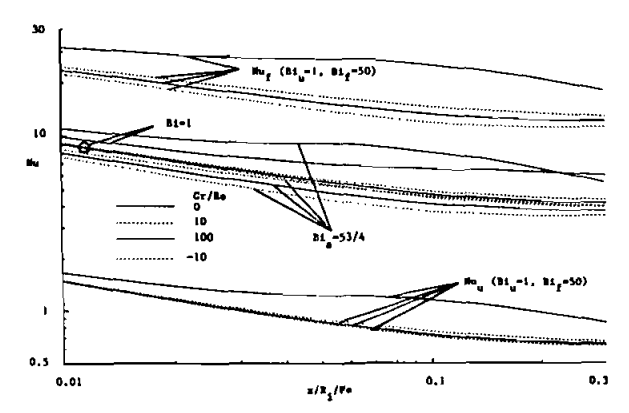


Figure 7. Streamwise variation of Nusselt number for axially periodic and constant Biot number values (Bi<sub>u</sub> = 1, Bi<sub>f</sub> = 50,  $\tau = 10^{-4}$ ,  $\sigma = 3\tau$ , and  $\kappa = \infty$ ).

are presented in Figures 7-9. These curves were drawn by calculating the average values of the Nusselt number  $\mathrm{Nu_u}$  in the unfinned sections and  $\mathrm{Nu_f}$  in the finned sections, and then connecting the respective values by smooth curves to provide continuity. The Nu curves, corresponding to the unfinned sections, indicate lower heat transfer rates. This behavior is anticipated, since the fluid entering an unfinned section is preheated in the preceding finned section. All curves in Figures 7-9 (except those for which  $\mathrm{Gr/Re}=100$ ) exhibit a similar behavior of decreasing in the streamwise direction (with increasing fluid bulk temperatures) until they reach a constant value. Once this occurs, the thermally fully developed regime is attained. It should be mentioned here that thermally fully developed profiles were obtained within  $x/R_i/\mathrm{Pe} \leq 0.3$  for all cases presented except for the cases when  $\mathrm{Gr/Re}=100$ .

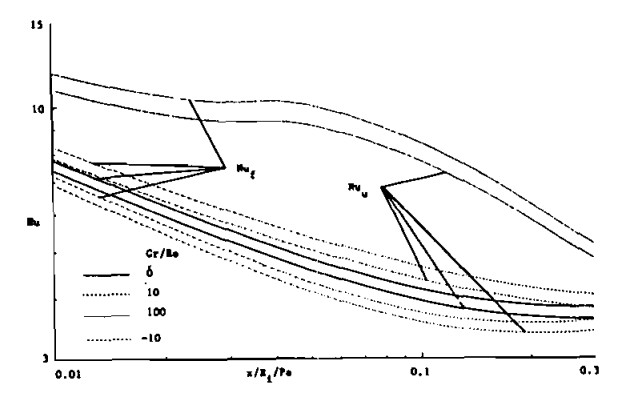


Figure 8. Streamwise variation of Nusselt number for axially periodic Biot number values (Bi<sub>u</sub> = 1, Bi<sub>f</sub> = 50,  $\tau = 10^{-4}$ ,  $\sigma = 3\tau$ , and  $\kappa = 16.5 \times 10^{-3}$ ).

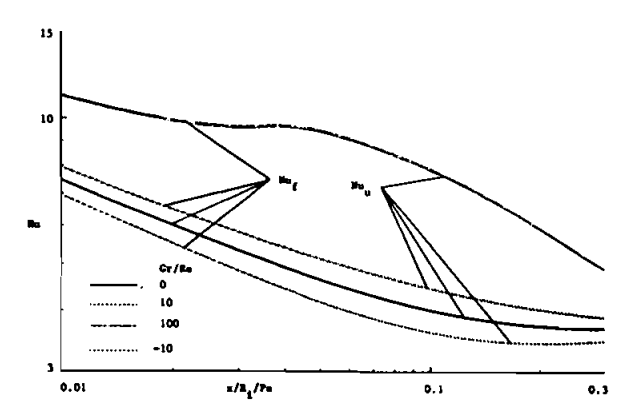


Figure 9. Streamwise variation of Nusselt number for axially periodic Biot number values (Bi<sub>u</sub> = 1, Bi<sub>f</sub> = 50,  $\tau = 10^{-4}$ ,  $\sigma = 3\tau$ , and  $\kappa = 1.65 \times 10^{-3}$ ).

The effects of the pipe wall thermal conductivity on the streamwise distribution of Nu can be observed by comparing the results in Figures 8 and 9 with those in Figure 7. As longitudinal conduction increases, wall temperatures become more uniform, that is, the wall temperatures in the finned segments decrease and those in the unfinned segments increase. Thus, correspondingly, the Nu differences between the finned and unfinned segments decrease. In Figure 9 the Nu, and Nu, curves are very close and nearly overlap each other. In all cases, the lowest of Nu, and  $Nu_f$  curves are for Gr/Re = -10 (downward flow), while the highest curves are for Gr/Re = 100, for reasons explained earlier. Moreover, for Gr/Re = 100 the Nu<sub>u</sub> and Nu<sub>f</sub> curves show a peak (near  $x/R_i/Pe = 0.08$  for the case of no conduction in the pipe wall (Figure 7) and in the neighborhood of  $x/R_i/Pe = 0.04$ for the cases when the pipe wall conductivity is taken into consideration (Figures 8 and 9)) and then decrease toward the periodically fully developed values. This peak is due to a sufficiently strong acceleration of the flow near the pipe wall, as will be discussed in the next section, which causes a large enough increase in the tube-side convection heat transfer coefficient to offset the decrease due to boundary layer growth. The shift in the location of the peak upstream toward the pipe inlet, for cases when the wall conductivity is finite, is due to preheating of the pipe wall by axial conduction, which causes the flow acceleration to occur further upstream. Also shown in Figure 7, for reference purposes, are the local Nu for the constant Bi of 1 and 53/4, whose streamwise distribution is expectedly seen to lie between the Nu and Nu curves.

Table 1 presents, for one set of Bi and  $\sigma$  and  $\tau$  values, the axially averaged Nu for the finned and unfinned sections of the pipe, defined by

$$\overline{Nu_{u}} = \frac{\sum_{i} Nu_{u}(x_{i})\sigma}{\sum_{i} \sigma} \qquad \overline{Nu_{f}} = \frac{\sum_{j} Nu_{f}(x_{j})\tau}{\sum_{j} \tau}$$
(10)

The average Nu trends are in keeping with the local profiles presented earlier:  $\overline{Nu_u}$  increases substantially, and  $\overline{Nu_f}$  decreases to a lesser extent when  $\kappa$  changes from

Gr/Re	$Bi_u = 1$ , $Bi_f = 50$ , $\tau = 10^{-4}$ , and $\sigma = 3\tau$				Bi = 1		$Bi_a = 53/4$		
	$\kappa \times 10^3$	Nu	Nuf	Nu <sub>u,pd</sub>	Nu <sub>f,pd</sub>	Nu	Nu <sub>pd</sub>	Nu	Nu <sub>pd</sub>
- 10		0.9292	12.109	0.7342	10.41	4.87	3.962	4.154	3.502
	16.5	3.945	4.099	3.384	3.553	4.021	3.44	3.98	3.423
	1.65	3.96	3.973	3.418	3.434	3.981	3.423	3.976	3.422
0	∞	0.9452	13.255	0.7482	11.28	5.059	4.159	4.502	3.752
	16.5	4.285	4.486	3.617	3.83	4.373	3.686	4.331	3.667
	1.65	4.314	4.323	3.661	3.681	4.332	3.666	4.327	3.665
10	∞	0.9712	14.392	0.7682	12.06	5.246	4.356	4.861	3.982
	16.5	4.639	4.886	3.816	4.055	4.739	3.879	4.697	3.871
	1.65	4.683	4.689	3.864	3.886	4.698	3.87	4.693	3.868
100	∞	1.2642	22.693	0.9512	17.07	6.794	5.983	7.59	5.434
	16.5	7.172	7.741	4.833	5.185	7.396	5.02	7.303	4.891
	1.65	7.248	7.306	4.877	4.908	7.309	4.897	7.295	4.881

Table 1. Average and fully developed Nusselt number values

 $\infty$  to  $16.5 \times 10^{-3}$ . Between  $\kappa$  of  $16.5 \times 10^{-3}$  and  $1.65 \times 10^{-3}$ ,  $\overline{Nu_u}$  and  $\overline{Nu_f}$  change by a comparable amount. The same behavior applies to the periodically fully developed Nu for the unfinned  $(\overline{Nu_u})$  and finned  $(\overline{Nu_f})$  portions of the tube. In long pipes the use of the periodically developed values is expected to be a reasonable representation of the average value. Also included in Table 1, for completeness of presentation, are the average and fully developed values for the uniform Bi cases.

#### **VELOCITY DISTRIBUTION**

The axial velocity profiles at four different cross-stream locations along the pipe, for the case when  $Bi_u = 1$ ,  $Bi_f = 50$ ,  $\tau = 10^{-4}$ ,  $\sigma = 3\tau$ , and for the various values of  $\kappa$ , are depicted in Figure 10. The velocity profiles for small  $x/R_i/Pe$ (= 0.01) are only slightly different from those of the pure forced convection profiles, with the largest deviation at the largest Gr/Re and the pipe wall conductivity values. Further downstream, the deviation in the forced convection profiles is much higher. Taking first the cases of positive Gr/Re, at any k value, the centerline velocity tends to decrease downstream, reaches a minimum, and then increases again. This is due to the acceleration of the near-wall fluid by buoyancy forces. Since the mass flow rate is constant, the velocity in the neighborhood of the centerline must be correspondingly lower. However, increasing flow velocities are associated with increasing viscous effects, and as  $x/R_i$ /Pe increases, the fluid bulk temperature also increases, and the local buoyancy-induced acceleration decreases. Thus, with streamwise development of the flow, the buoyant forces, the viscous retardation, and the pressure forces start to balance each other, driving the velocity profile toward its fully developed state. Beyond a certain X, due to radial diffusion, the centerline velocity starts to rise again. The above described effect is more pronounced for Gr/Re = 100, where the maximum velocity shifts toward the pipe wall, and a concavity in the velocity profile (associated with depressed centerline velocity) develops around the centerline.

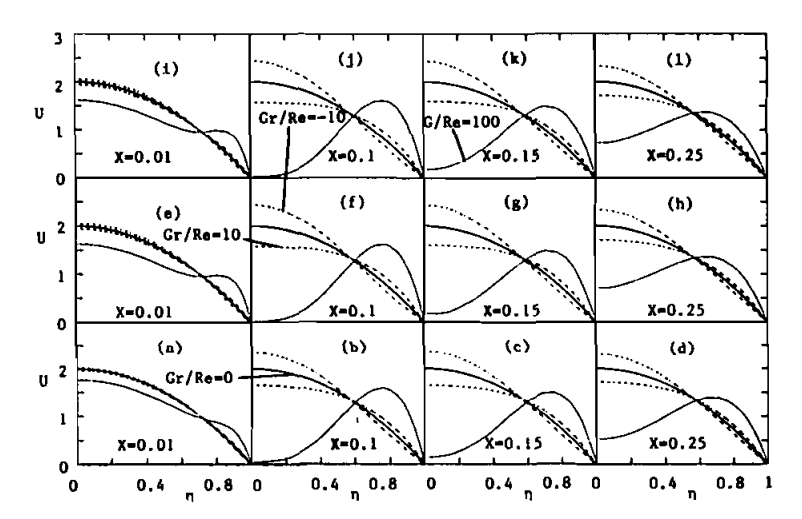


Figure 10. Velocity profiles at various axial stations and for different Gr/Re values (Bi<sub>u</sub> = 1, Bi<sub>f</sub> = 50,  $\tau = 10^{-4}$ ,  $\sigma = 3\tau$ ): (a-d)  $\kappa = \infty$ , (e-h)  $\kappa = 16.5 \times 10^{-3}$ , and (i-l)  $\kappa = 1.65 \times 10^{-3}$ .

For negative values of Gr/Re, the opposite effect is observed. At moderate  $x/R_i/Pe$  stations, buoyancy effects are strong and retard the flow close to the wall. In order for continuity to be satisfied, the centerline velocity increases. As the difference between the fluid and wall temperatures diminishes, these effects decrease in magnitude, the centerline velocity starts to decrease, and the velocity eventually reaches the fully developed state.

The effect of the pipe wall thermal conductivity is to accentuate the above noted behavior. Since, due to axial conduction, there is greater heat transferred to the fluid, and buoyancy effects are enhanced, for positive Gr/Re, the near-wall acceleration of the flow is enhanced, and for negative Gr/Re, the near-wall deceleration of the flow is greater with increasing wall conductivity. Stronger buoyancy in the early development stages of the flow leads to a faster recovery of the fully developed profile (compare Figures 10d, 10h, and 10l). For a pipe of poorly conducting material ( $\kappa = \infty$ ), the smaller levels of heat transferred to the flow cause a more gradual development in these profiles.

The centerline velocity increases with Gr/Re when buoyancy is in the opposing mode (Gr/Re < 0) and decreases when it is in the aiding mode (Gr/Re > 0). For Gr/Re = 100 the centerline velocity decreases to a near-zero value. Experimentation with values of Gr/Re > 100 caused negative centerline velocities and separation of the flow that cannot be handled with the parabolic solution technique adopted in this work.

#### TEMPERATURE DISTRIBUTION

The temperature profiles presented in Figure 11 reflect the streamwise variation of the fluid bulk temperature. As shown, the temperatures increase

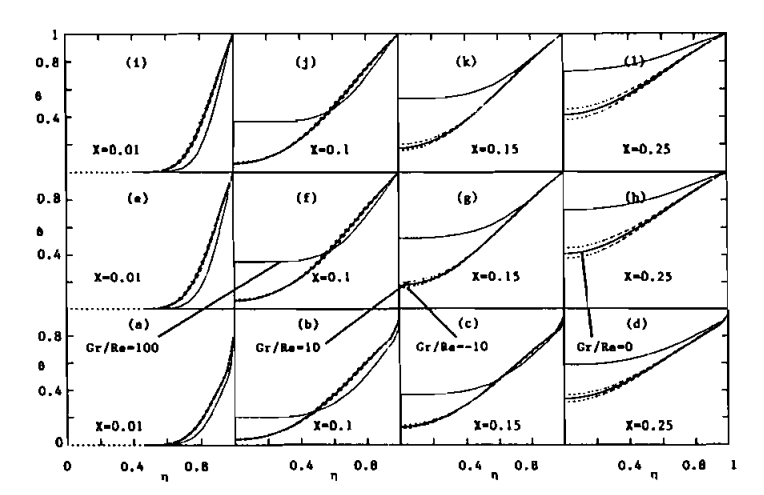


Figure 11. Temperature profiles at various axial stations and for different Gr/Re values (Bi<sub>u</sub> = 1, Bi<sub>f</sub> = 50,  $\tau = 10^{-4}$ ,  $\sigma = 3\tau$ ):  $(a-d) \kappa = \infty$ ,  $(e-h) \kappa = 16.5 \times 10^{-3}$ , and  $(i-l) \kappa = 1.65 \times 10^{-3}$ .

downstream and do so faster at a higher value of Gr/Re and higher values of wall conductivity. This is again linked to stronger buoyancy effects at the higher parameter values, which cause stronger near-wall acceleration of the flow and higher temperature gradients during the initial development of the flow.

Typical streamwise variations of the pipe wall temperature are presented in Figures 12 and 13. The high wall conductivity curves exhibit a smoother variation due to the smoothening effect of axial conduction in the pipe wall, the variation becoming increasingly less smooth at higher Gr/Re values. The maximum smoothening is obtained with the largest external heat transfer coefficients (Figure 13), where the pipe wall conduction has the strongest effect, and the wall tempera-

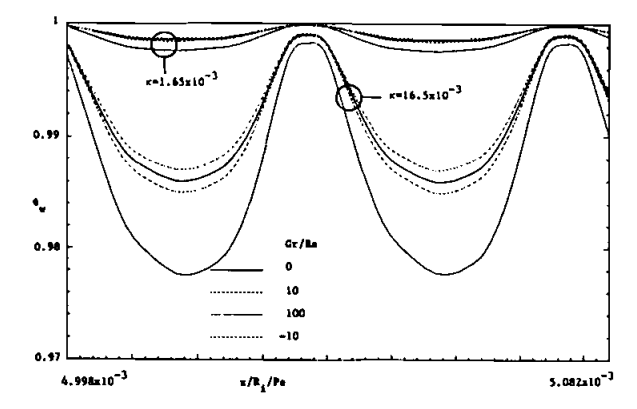
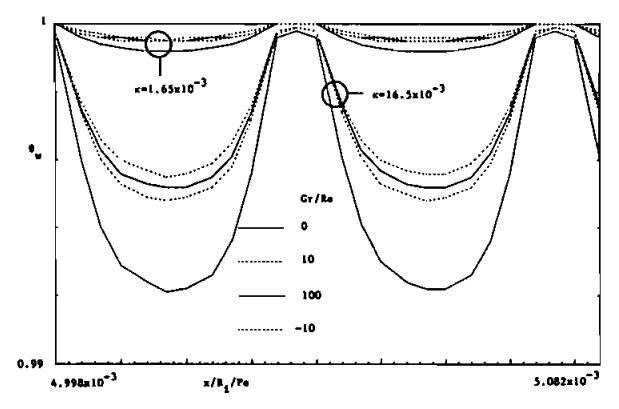


Figure 12. Pipe wall temperature distribution for  $4.998 \times 10^{-3}$   $< x/R_i/Pe < 5.082 \times 10^{-3}$  (Bi<sub>u</sub> = 1, Bi<sub>f</sub> = 50,  $\tau = 10^{-4}$ , and  $\sigma = 3\tau$ ).



**Figure 13.** Pipe wall temperature distribution for  $4.998 \times 10^{-3} < x/R_i/Pe < 5.082 \times 10^{-3}$  (Bi<sub>u</sub> = 5, Bi<sub>f</sub> = 250,  $\tau = 10^{-4}$ , and  $\sigma = 3\tau$ ).

tures are closer to  $T_{\infty}$  (note the vertical scale in Figure 13 is considerably smaller in range than that in Figure 12). With decreasing wall conductivity values, the smoothening effect of axial conduction is reduced, and the temperature curves show a highly nonmonotonic periodic variation. The amplitude of these variations increases with decreasing external heat transfer coefficient and increasing Gr/Re values. Increasing the interfin spacing, which reduces the effect of axial conduction, expectedly leads to temperature variations of larger amplitude and larger wavelength.

#### CONCLUSION

A numerical investigation is conducted of conjugate conduction-mixed convection heat transfer in externally finned vertical pipes. The effects of wall conductivity, interfin spacing, buoyancy forces, and external heat transfer coefficient are examined. Axial conduction in the pipe wall is found to strongly affect the flow and thermal fields. Buoyancy effects are stronger when the pipe wall conductivity is considered, and increase the overall heat transferred to the fluid if buoyancy is in the aiding mode and decrease it if buoyancy is in the opposed mode. Longitudinal wall conduction (and therefore, the buoyancy) is reduced with decreasing wall conductivity, increasing interfin spacing, and decreasing levels of the external heat transfer coefficient (which represents the fin surface area). Nusselt numbers and wall temperatures in the finned and unfinned regions show significant differences in their respective magnitudes, but these differences diminish with increasing conduction on the longitudinal wall. An approximation of the area-averaged Biot number can significantly overestimate the heat transferred if wall conductivity is zero or small, but this overestimation diminishes to less than 10% at higher wall conductivities. Buoyancy decelerates the near-wall flow in the opposed mode and, consequently, reduces the near-wall temperatures. In the aiding mode, buoyancy accelerates the near-wall flow that, in turn, causes centerline velocities to be depressed.

#### REFERENCES

- 1. E. M. Sparrow and M. Charmchi, Laminar Heat Transfer in an Externally Finned Circular Tube, ASME J. Heat Transfer, vol. 102, pp. 605-611, 1980.
- F. Moukalled and S. Acharya, Forced Convection Heat Transfer in a Finitely Conducting Externally Finned Pipe, ASME J. Heat Transfer, vol. 110, pp. 571-576, 1988.
- 3. F. Moukalled, J. Kasamani, and S. Acharya, Turbulent Convection Heat Transfer in Longitudinally Conducting, Externally Finned Pipes, *Numer. Heat Transfer Part A*, vol. 21, pp. 401-421, 1992.
- 4. F. Moukalled, M. Darwish, and S. Acharya, Laminar Mixed Convection Heat Transfer in Externally Finned Pipes, J. Enhanced Heat Transfer, 1995 (in press).
- 5. Y. K. Lin and L. C. Chow, Effects of Wall Conduction on Heat Transfer for Turbulent Flow in a Circular Tube, ASME J. Heat Transfer, vol. 106, pp. 597-604, 1984.
- M. Faghri and E. M. Sparrow, Simultaneous Wall and Fluid Axial Conduction in Laminar Pipe-Flow Heat Transfer, ASME J. Heat Transfer, vol. 102, pp. 58-63, 1980.
- N. K. Anand and D. R. Tree, Some Studies of the Effects of Axial Conduction in a Tube Wall on the Steady State Laminar Convective Heat Transfer, ASME J. Heat Transfer, vol. 109, pp. 1025-1028, 1987.
- 8. R. M. Fithen and N. K. Anand, Finite Element Analysis of Conjugate Heat Transfer in Axisymmetric Pipe Flows, *Numer. Heat Transfer*, vol. 13, pp. 189-203, 1988.
- G. S. Barozzi and G. Pagliarini, A Method to Solve Conjugate Heat Transfer Problems: The Case of Fully Developed Laminar Flow in a Pipe, ASME J. Heat Transfer, vol. 107, pp. 77-83, 1985.
- H. M. Soliman, Analysis of Low Péclet Heat Transfer During Slug Flow in Tubes with Axial Wall Conduction, ASME J. Heat Transfer, vol. 106, pp. 782-788, 1984.
- 11. E. K. Zariffeh, H. M. Soliman, and A. C. Trup, The Combined Effects of Wall and Fluid Axial Conduction on Laminar Heat Transfer in Circular Tubes, *Proc. 7th Int. Heat Transfer Conf.*, vol. 88, pp. 131-135, 1985.
- 12. W. T. Lawrence and J. C. Hato, Heat Transfer Effects on the Developing Laminar Flow Inside Tubes, ASME J. Heat Transfer, vol. 88, pp. 214-222, 1966.
- W. J. Marner and H. K. McMillan, Combined Free and Forced Laminar Convection in a Vertical Tube with Constant Wall Temperature, ASME J. Heat Transfer, vol. 92, pp. 559-562, 1970.
- M. W. Collins, Combined Convection in Vertical Tubes, Symposium on Heat and Mass Transfer by Combined Forced and Natural Convection, Paper C155/71, Institution of Mechanical Engineers, London, UK, 1971.
- B. Zeldin and F. W. Schmidt, Developing Flow with Combined Forced-Free Convection in an Isothermal Vertical Tube, ASME J. Heat Transfer, vol. 94, pp. 211-223, 1972.
- B. Morton, D. B. Ingham, D. J. Kenn, and P. J. Heggs, Recirculating Combined Convection in Laminar Pipe Flow, ASME J. Heat Transfer, vol. 111, pp. 106-113, 1989.
- P. J. Heggs, D. B. Ingham, and D. J. Keen, The Effects of Heat Conduction in the Wall on the Development of Recirculating Combined Convection Flows in Vertical Tubes, Int. J. Heat Mass Transfer, vol. 333, pp. 517-528, 1990.
- M. A. Bernier and B. R. Baliga, Conjugate Conduction and Laminar Mixed Convection in Vertical Pipes for Upward Flow and Uniform Wall Heat Flux, Numer. Heat Transfer Part A, vol. 21, pp. 313-332, 1992.
- S. V. Patankar and D. B. Spalding, Heat and Mass Transfer in Boundary Layers, Intertext Books, London, 1970.
- S. V. Patankar, Numerical Heat Transfer and Fluid Flow, Hemisphere, Washington, D. C., 1980.